IIT, Madras

Hot deformation characteristics and microstructure evolution of Ti–5Al–3Mo–1.5V alloy

Faisal Waqar Syed[1] · Nitesh Raj Jaladurgam[2] · V. Anil Kumar[3] · Rohit Kumar Gupta[3] ·
Anand K. Kanjarla[1]

Abstract A detailed investigation was conducted to study the concurrent effect of temperature and strain rate on the microstructure evolution in Ti–5Al–3Mo–1.5V dual-phase Titanium alloy. By applying varying strain rates from 10^{-3} to 10 s^{-1} between 1098 and 1298 K at an interval of 50 K, isothermal compression characteristics and microstructural changes were recorded. The sizes of globules, concentrated predominantly at the lamellar kinks, were found to be inversely proportional to the strain rate. Further, a dynamic material model was employed to assess and plot the processing map displaying the safe hot working regime. The apparent hot-working activation energy in the $\alpha + \beta$ and β phase field was 636 kJ/mol and 379 kJ/mol, respectively. A higher activation energy than the self-diffusion threshold of the $\alpha + \beta$ and β field was attributed to lamellae breakup and dynamic recrystallization in the respective phase fields. The microstructure analysis and identified softening mechanisms further helped in concluding the safe hot working regime to be 1248 K and 10^{-3} s^{-1}.

1 Introduction

Ti–5Al–3Mo–1.5V is a two-phase high-strength structural titanium alloy. Its prowess to withstand high strain prior to failure in annealed or quenched state has been widely reported [1]. The alloy undergoes structure change from HCP to BCC while heating at a temperature of 1223 K (β transus, T_β). Post-solution treatment and ageing, the alloy exhibits satisfactory strength up to a temperature of 673–703 K and presents better properties than Ti–6Al–4V; viz. enhanced strength and moderate ductility. Weldments and forged structure of this alloy can be deployed in service for long span at temperatures up to 673 K and short span up to 1023 K [1]. However, there has been very little reported work exploring the high-temperature mechanical performance of the alloy.

Microstructural features have been known to influence the mechanical behaviour of titanium alloys. For example, grain refinement in metals is a widely accepted approach for enhancing mechanical properties. A change in the lamellae thickness has been reported to manifest itself in the form of tension/compression asymmetry during the mechanical test of this alloy [2]. Hot working studies on Ti–6Al–4V maintained that globularization (lamellar → globular) kinetics were significantly influenced by initial microstructure [3]. Although the lamellar structure is stable up to high temperature due to the absence of

✉ Anand K. Kanjarla
kanjarla@iitm.ac.in

Faisal Waqar Syed
sfwaqar@gmail.com

Nitesh Raj Jaladurgam
niteshj@chalmers.se

V. Anil Kumar
anilkumar_v@vssc.gov.in

Rohit Kumar Gupta
rohitkumar_gupta@vssc.gov.in

1 Department of Metallurgical and Materials Engineering, IIT Madras, Chennai, India

2 Department of Physics, Chalmers University of Technology, 41296 Gothenburg, Sweden

3 Vikram Sarabhai Space Centre, Indian Space Research Organization (ISRO), Trivandrum, India

interface curvature; it was established that the presence of defects like lamellar termination and lamellar boundaries have detrimental effect [4]. Furthermore, it was concluded that with suffcient thermal energy and deformation, production of perturbation and further breakdown of lamellar microstructure results in globular or equiaxed morphology [5]. Mechanistic models presented in [4] and [6] describing the mechanism involved in the transformation of lamellar to globular/equiaxed morphology, albeit primarily for static globularization, stressed on lamellar termination migration, boundary splitting and Rayleigh perturbation theory-based capillarity-induced instabilities.

The height reduction required during hot compression to achieve dynamic globularization for lamellar microstructure is approximately 50%. It was argued that the strain path is also expected to have a profound effect on the globularization kinetics. Monotonic deformations (e.g. tension and torsions) present higher rates of globularization than the reversed torsion types non-monotonic ones [7]. Intense shear bands formation within alpha colony precede the globularization process. It was maintained that the development of this high energy alpha–alpha interfaces in the vicinity of beta lamellae results in a surface-tension-induced perturbation of the alpha lamellae by beta lamellae [8]. Recent studies on the hot working of Ti–6Al–4V reported that for strain rates lesser than 10^{-2} s^{-1} globularization occurred below β-transus while dynamic recrystallization (DRX) took place above the transus temperature [9]. DRX has been regarded as a softening mechanism that leads to the evolution of new finer grains in the existing matrix, which further helps to enhance mechanical properties post-hot working [10]. It was further argued that a certain threshold strain was necessary to initiate DRX [11]. Subsequently, a quantitative model was employed comprising cellular automata coupled with DRX metallurgical principles and concluded that grain boundaries successfully overcame the threshold and act as preferred sites for nucleation of these fine grains [12]. Kugler and Turk [13] also utilized cellular automata and maintained that migration of dislocation-rich high angle grain boundaries into the surrounding matrix brings about the formation of fine dislocation-free new grains. Experimental kinetic analysis for lamellar starting microstructure in TC11 titanium alloy has suggested that the deformation mechanism in the β phase field was governed by diffusion creep process, and microstructure evolution was a combination of dynamic recovery and dynamic recrystallization [14].

The present work reports the effect of deformation parameters on the microstructural evolution in two-phase Ti–5Al–3M–1.5V Titanium alloy for lamellar starting microstructure. By employing TEM and OM, an attempt has been made to understand the globularization (below T_β) and recrystallization (above T_β) mechanism in the ensuing deformation.

2 Material and experiment

2.1 Material

The alloy used in the current study, with similar elemental composition and history as reported in [2], was subjected to solutionization at 1253 K for 45 min, followed by furnace cooling to ambient temperature to achieve lamellar morphology. Figure 1 depicts the lamellar microstructure obtained after furnace cooling. The α and the β phases are represented by dark and bright regions, respectively. The microstructure is comprised of colonies of lamellar α within the prior β grain. Prominent grain boundary α layer is visible along with continuous β layer in between Widmanstätten side plates.

2.2 Hot compression and microstructure examination

Isothermal hot compression tests were conducted on cylindrical specimens of 12-mm length and 8-mm diameter on the Gleeble thermomechanical simulator. Tests were conducted for the temperature range of 1098–1298 K at an interval of 50 K each for true strain rates of 10^i s^{-1} (i = 0.001, 0.01, 0.1, 1.0, 10.0). The specimens were resistance heated to the test temperature at a heating rate of 278 K s^{-1} and homogenized for 180 s and subsequently water quenched after 50% deformation to retain the hot-worked microstructure. Standard metallographic technique mentioned for this alloy in [2] was adopted to prepare specimens for microstructural examination.

3 Results and discussion

Following the mentioned outline in the introduction, firstly, the stress–strain profile variation with temperature and strain rate is discussed. Further on microstructure evolution mechanisms in below and above β-transus, hot working at different strain rates is illustrated.

Fig. 1 OM image of starting lamellar microstructure at **a** lower magnification and **b** higher magnification.
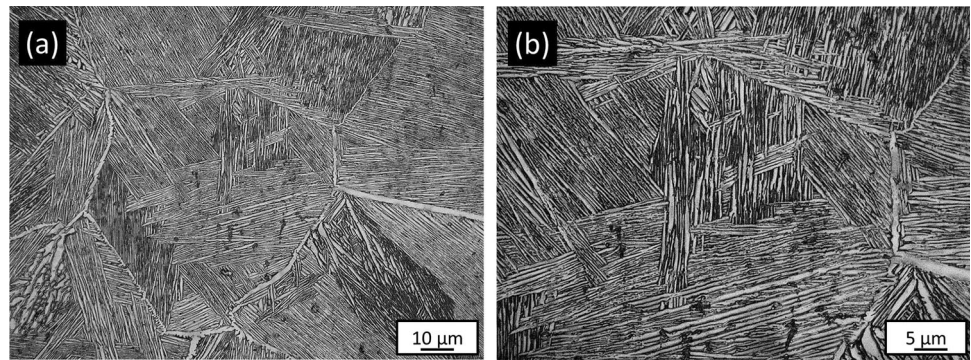
3.1 Stress–strain profile—flow behaviour

The shape of true stress versus true strain curves (Fig. 2a–e) for the high-temperature compression of the alloy for varying temperatures and strain rates can be distinguished into the following categories:

1. For temperatures 1098 and 1148 K, after peak stress attainment, continuous flow softening was witnessed up to true strain value of 0.4.
2. For strain rates higher than 0.01 for below β transus test temperatures, a drastic drop in flow stress with increasing strain was observed
3. For temperatures just below β transus, i.e. 1198 K, a at stress–strain profile was observed only for 0.001 s^{-1} strain rate, in the rest (0.1–10.0 s^{-1}) drastic fall in flow stress with the increasing strain was observed.
4. For above β transus specimens, a flat stress–strain profile was observed.

Reported literature has stressed on the incapability of texture change, dislocation substructure and dynamic globularization to cause flow softening [15, 16]. Plate/lamellae kinking, which is prevalent in below β transus hot-worked specimens, can be considered a plausible cause of flow softening [17]. Just as the plastic buckling of beams leads to load drop, kinking can also cause deformation under decreasing loads (the constraints in the deformation of the lamellar microstructure are more complex than simple beam). A parallel study conducted on Ti–6Al–4V stressed on the adiabatic heating during deformation in the two phase $(\alpha + \beta)$ regime as a probable cause for flow softening. Adiabatic heating increases the specimen temperature. The study further described the flow stress as a function of temperature and strain rate and established a converse correlation between flow stress and deformation. For hot deformation near or above β transus, the flow stress exhibited a constant profile. This is due to the dynamic recovery and recrystallization phenomena [18].

### 3.2 Deformed microstructural analysis

3.2.1 Deformed microstructure—lower two-phase $\alpha + \beta$ region

Globularization of the lamellar α was the major microstructural change witnessed during deformation at temperatures 1098, 1148 K at 10^{-3} s^{-1} strain rate. Figure 3 shows the micrographs of specimens deformed at the aforementioned conditions. Formation of primary equiaxed α (black square marked 'J' (Fig. 3a, b) after globularization is clearly evident from the images. Globularization was preferential and concentrated at the lamellae kink and prior β grain boundaries as has been reported previously [3, 19]. The modification in the aspect ratio of the α lamellae can be understood by the concept of geometric recrystallization [20]. The appearance of steps or grooves [black square marked 'I' (Fig. 3a, b)] over the parallel α colony either by surface tension or by strain localization help in lamellae fragmentation and their transformation to equiaxed morphology [15].

3.2.2 Globularization mechanism

The globularization mechanism of α lamellae consisted of two phenomena: shearing/kinking of laths and formation of globules. Figure 4a shows the kinking contour of lamellae and subsequent formation of globules at the kinks (marked by arrows). Shearing of lath by plastic deformation creates dislocations of both signs along the shearing plane. High-temperature deformation results in simultaneous recovery by the annihilation of oppositely signed dislocations. Remaining dislocations of similar sign nucleate an interface along shear line. The formation of these intra-lamellae interfaces prior to globularization has been previously reported for TA15 titanium alloy albiet for interrupted compression test [21]. Squares marked with label K and L highlighting the interface formation inside the lamellae in specimens deformed at 1098 K at a strain rate of 0.001 and

Fig. 2 Flow curves of Ti–5A–3Mo–1.5V at different strain rates in the **a** $\alpha + \beta$ range (1098, 1148,1198 K) and **b** β range (1248, 1298 K

(a) 1098 K

(b) 1148 K

(c) 1198 K

(d) 1248 K

(e) 1298 K
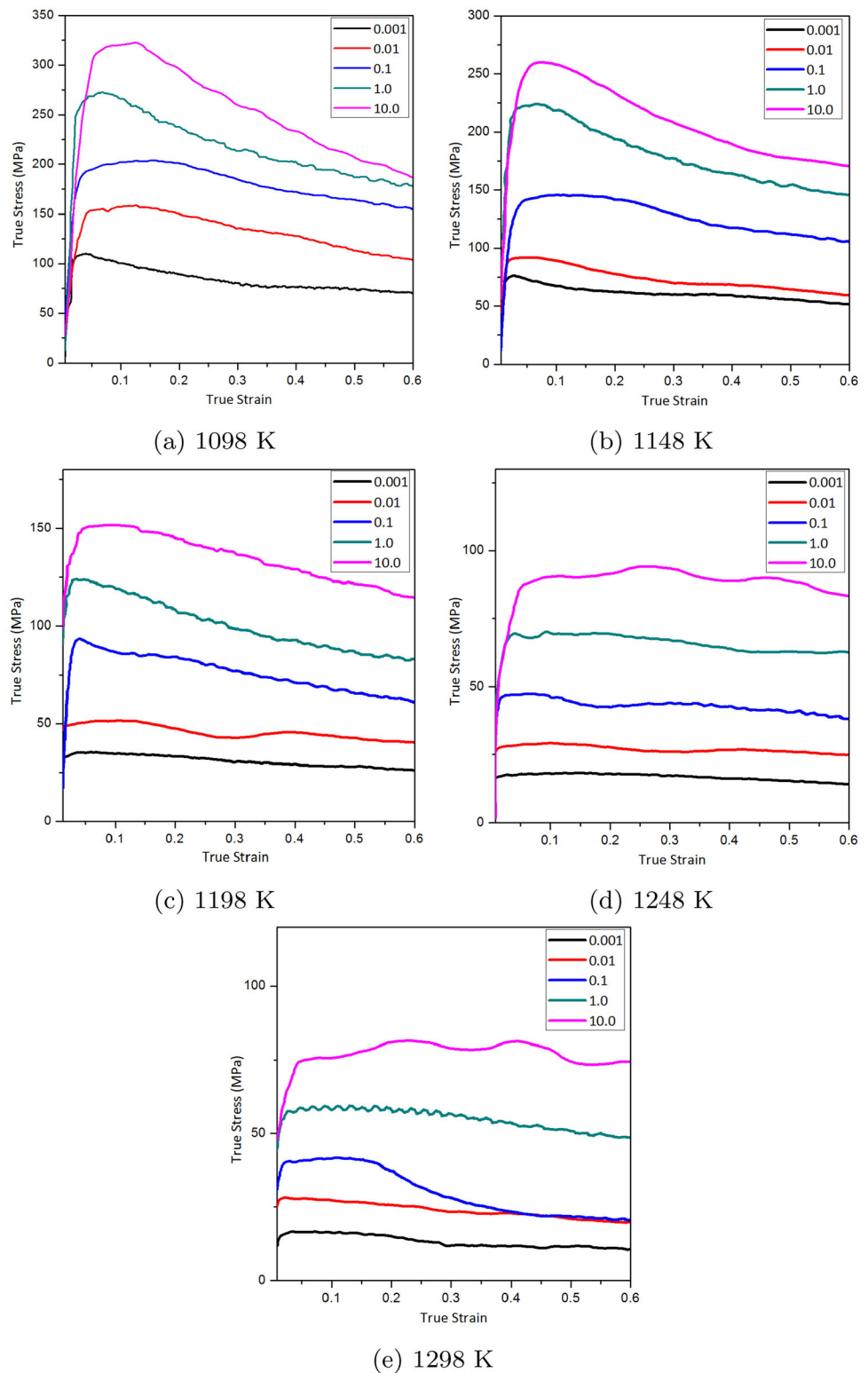
$0.1s^{-1}$, respectively, are shown in Fig. 4b, c. This interface diffuses and forms a globular shape to minimize the interfacial energy (Marked J in Fig. 4b). The globule then further grows to what is called an equiaxed morphology (Marked I in Fig. 4b). Globularization near the prior β grain boundaries is due to the higher local strains or the stress arising because of deformation incompatibilities between alpha lamellae and grain boundary. The propensity of globularization near kinks is due to the plate bending, which results in intensified local strain/stress. The

(a) 1098 K   (b) 1148 K   (c) 1198 K
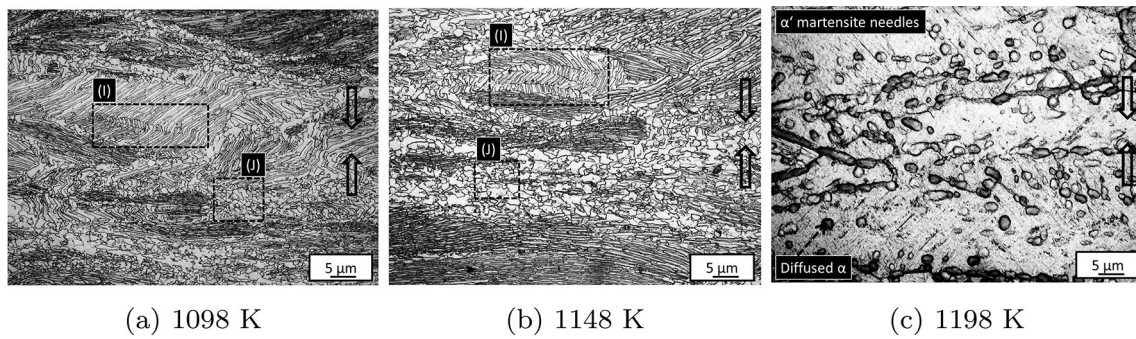
Fig. 3 Globularization in specimens deformed to 0.69 true strain at 1098, 1148, 1198 K at a strain rate of 10^{-3} s^{-1}. The compression axis is vertical
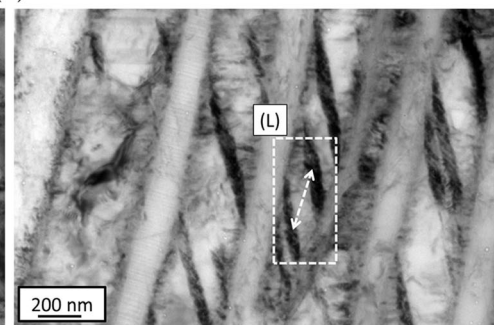
Fig. 4 Bright field TEM images of specimens deformed at 1098 K to 0.69 true strain at a strain rate of **a** 0.001s^{-1} showing lamellae kinking contour and globularized α, **b** 0.001s^{-1} showing progress of globularization (I and J) and pre-globularization fragment (K) and **c** 0.1s^{-1} showing pre-globularization fragment (L)
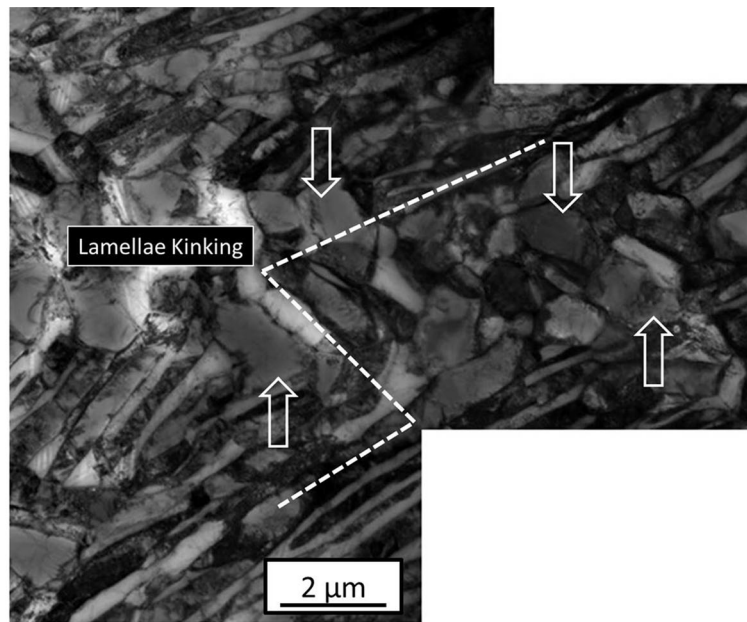
(a)
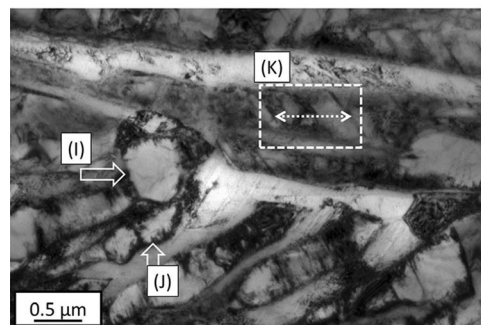
(b)   (c)

nonuniformity in deformation further worsens due to the absence of grain boundary sliding [3] as concluded from the values of strain rate sensitivity and strain components in previously reported works [15].

The observed rotation of large fraction of lamellae to an orientation orthogonal to the loading axis in this work (Fig. 5) and other previous work [15] at critical strain levels necessary for the inception of dynamic globularization is worth noticing. It further indicates that reorientation/ kinking of lamellae also manifests itself in critical strain needed for the commencement of globularization.

(a) T=1098 K, $\dot{\epsilon}=10^{-2}\mathrm{s}^{-1}$ (b) 1148 K, $\dot{\epsilon}=10^{-2}\mathrm{s}^{-1}$ (c) T=1198 K, $\dot{\epsilon}=10^{-2}\mathrm{s}^{-1}$

(d) T=1098 K, $\dot{\epsilon}=10^{-1}\mathrm{s}^{-1}$ (e) T=1148 K, $\dot{\epsilon}=10^{-1}\mathrm{s}^{-1}$ (f) T=1198 K, $\dot{\epsilon}=10^{-1}\mathrm{s}^{-1}$

(g) T=1098 K, $\dot{\epsilon}=1\mathrm{s}^{-1}$ (h) T=1148 K, $\dot{\epsilon}=1\mathrm{s}^{-1}$ (i) T=1198 K, $\dot{\epsilon}=1\mathrm{s}^{-1}$

(j) T=1098 K, $\dot{\epsilon}=10\mathrm{s}^{-1}$ (k) T=1148 K, $\dot{\epsilon}=10\mathrm{s}^{-1}$ (l) T=1198 K, $\dot{\epsilon}=10\mathrm{s}^{-1}$
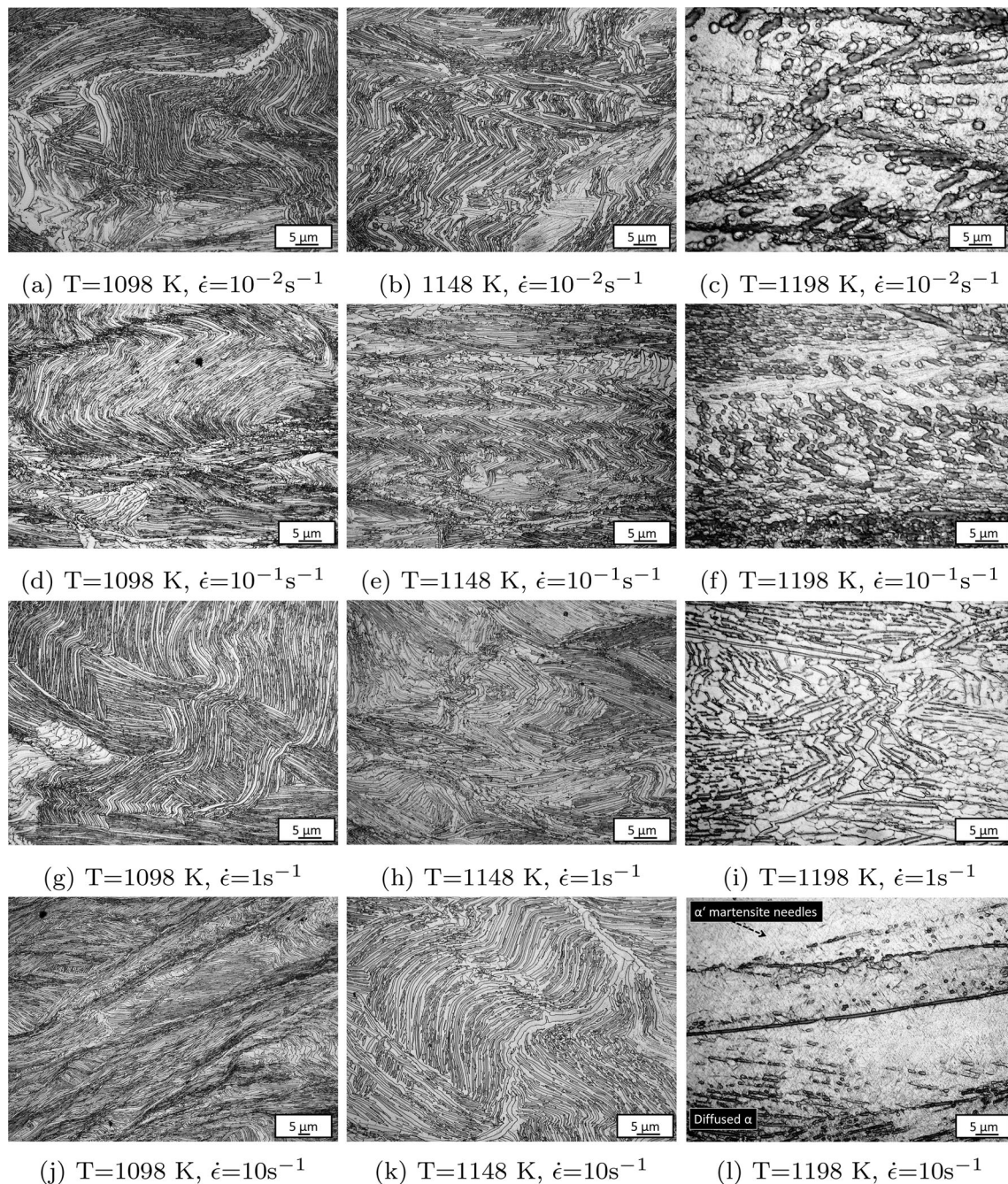
Fig. 5 OM images of microstructure of specimens deformed to 0.69 true strain exhibiting kinking and fragmenting of lamellae. The compression axis is vertical

3.2.3 Effect of strain rate on globularized grain size

As discussed earlier during the globularization process, the formation of grooves and steps on the alpha lamellae by surface tension or shear localization helps to fragment the lamellae by penetration of α phase. The diameter of the fragmented entity is usually equal to the thickness of the lamellae [20]. The lamellae fragmentation indeed takes place as mentioned, the size of globularized grain does not

necessarily be equal to the lamellae thickness. As can be seen from Fig. 4b, the discrepancy in the size of fragment 'J' and the globularized grain 'I'. The difference in the fragment sizes in specimens deformed at a strain rate of 10^{-3} and 10^{-1} s^{-1} for 1098 K can be seen from Fig. 4b and c, respectively. The length of the fragment in specimen deformed at 10^{-3} s^{-1} is larger than the lamellae thickness. Subsequently, the final globularized grain size larger than lamellae thickness can be readily expected. For specimens

deformed at 10^{-1} s^{-1}, the fragment size was comparable to the lamellae thickness. This difference in the aspect ratio of the fragment is a consequence of varying dynamic recovery rate at different strain rates. For lower strain rates, with fast recovery rate, dislocation annihilation and gliding is easier, resulting in less dense and distant dislocation wall formation. Higher strain rate results in the generation of more dislocations, and due to the poor rate of recovery, the dislocation walls are closer and denser. With the progress of deformation, the dislocation walls migrate to interphase boundaries and form fragments of varying aspect ratio. This is further conducive to different final globule sizes [22].

3.2.4 Microstructure evolution in upper two-phase $\alpha + \beta$ region

For the specimens hot worked at a temperature of 1198 K, the morphology of postdeformation α phase was different from those of 1098 and 1148 K. The microstructure shown in Fig. 3c is a typical example of diffused α. Our observation is consistent with the reports on the hot deformation of Ti–6Al–4V close to transformation temperature [18]. It appears as if the α lamellae have dissolved in the matrix during the heating process. The diffused zone is an outcome of an incomplete transformation, and if the holding time before deformation had been longer, it would have completely transformed to β phase. This partial β phase formed transforms to either secondary α or α' martensite upon quenching. One interesting observation was the occurrence of α' martensitic laths in the specimens deformed at 1198 K with a high strain rate of 10 s^{-1} (Fig. 5l). Considering high strain rate, it is expected that the time available for transformation will not be enough to create any discernible microstructural change. However, due to the high rate of deformation and very less time for heat dissipation, there is a high possibility of localized heating. With the operating temperature being close to the transformation temperature, local shoot up of temperature above the transus is expected, subsequently causing martensite evolution upon water quenching. The phase transformation ($\alpha \rightarrow \beta$) at high temperatures is a function of hot working temperature, strain rate, plastic deformation and microstructure of the specimen. It has been reported that the transformation ($\alpha \rightarrow \beta$) increases with increasing strain rate, further corroborating the assumption that plastic deformation close to β-transus induced the local phase transformation [23]. This would have further enhanced the percentage of α' martensite upon quenching.
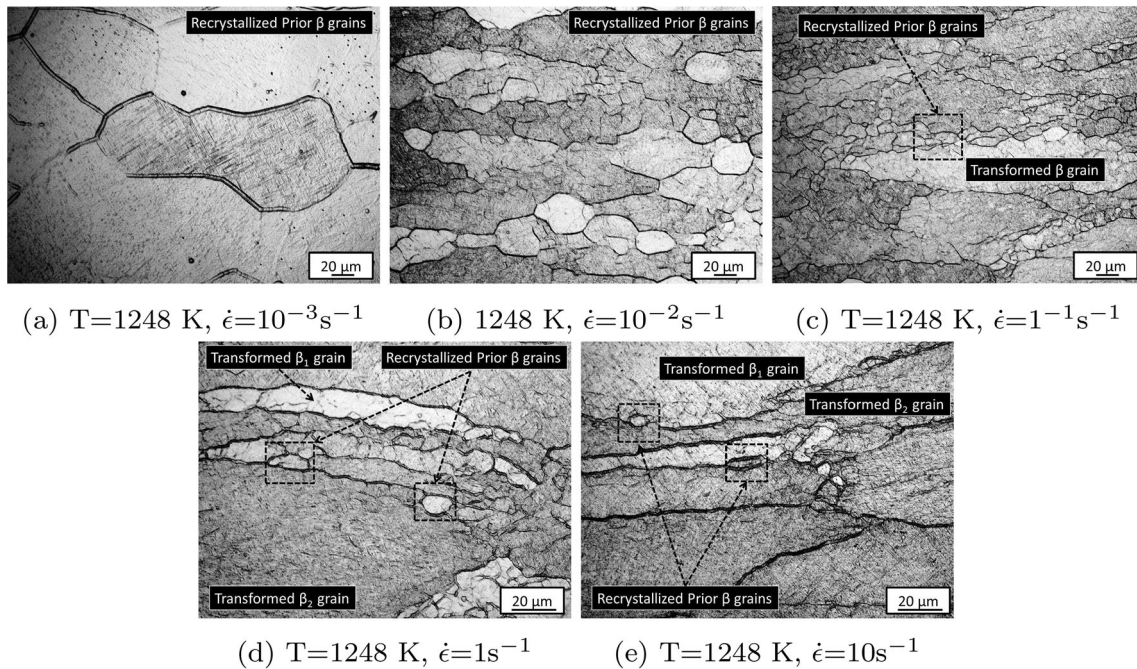
3.2.5 High strain rate deformed microstructure

Considerable globularization with globules extending till the interior of the grains was witnessed for low strain rate (10^{-3} s^{-1}), but beyond this, it was completely arrested. Specimens deformed at strain rates greater than 10^{-3} s^{-1} primarily exhibited kinking and fragmentation of lamellae at 45° angle to the loading axis (Fig. 5a–l). For specimen deformed at a temperature of 1098 K with a strain rate of 10 s^{-1}, localized flow bands were observed (Fig. 5j). With increased temperature of deformation and decreased strain rate, the intensity of these bands was seen to decrease. The occurrence of these flow bands is related to the low thermal conductivity of the alloy. Considering the high strain rate of deformation, the heat is not dissipated and reduces the local flow stress and thereby results in a localized flow [9]. Localized flow is detrimental for uniform mechanical properties and should be checked for during material processing.
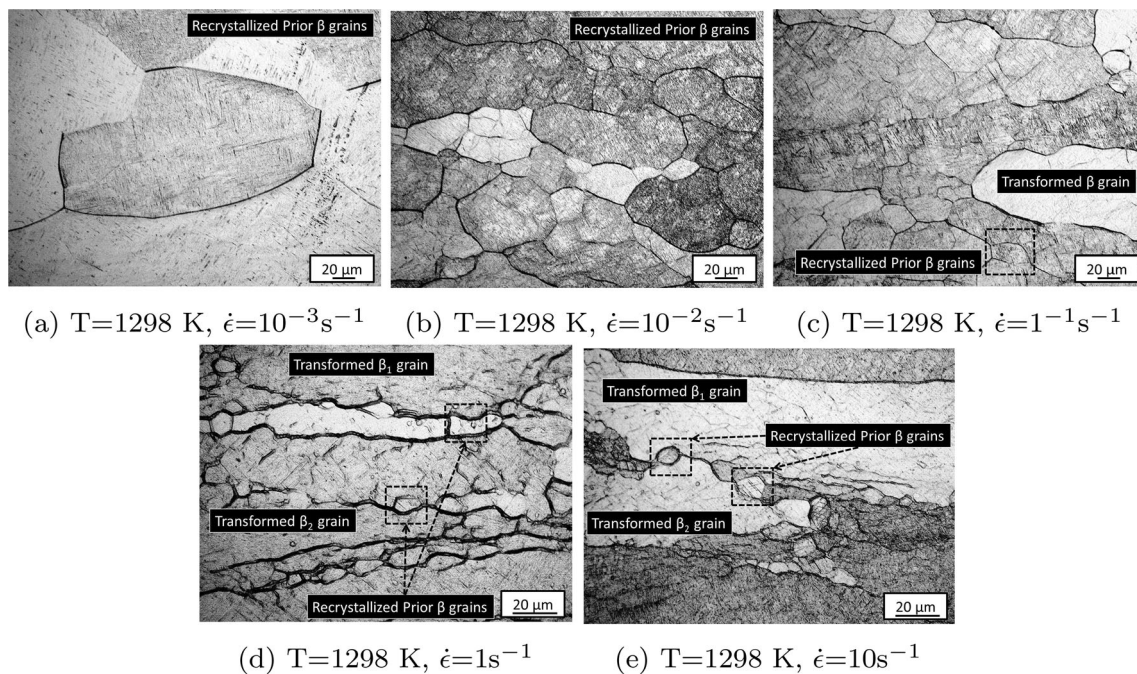
3.2.6 Deformation in the β region

Specimens hot worked above β transus consisted of a matrix of prior β grains with acicular martensite structure in the interior. Thus, it can be inferred that at hot working temperatures, microstructure must be only of single phase β and martensite would have formed as a result of fast cooling. The phase transformation during cooling from the single-phase regime hinders the exact interpretation of high-temperature deformation; some features are still recognizable. For hot working at a strain rate of 10^{-3} s^{-1} 1248 K, recrystallized equiaxed prior β grains with curved boundaries were seen. As the strain rate of deformation is increased to 10^{-2} s^{-1}, recrystallized prior beta grains decreased in size. The morphology of prior β grains became elongated with its boundaries appearing jagged and serrated with further increase in strain rate. The concurrent presence of transformed elongated β grains and serrated boundary hints towards strain-induced grain boundary migration; subsequently, dynamic recovery (DRV) is considered to be a major restoration mechanism for this deformation condition [24]. Finer equiaxed prior β grains (square brackets in Fig. 6c–e) were observed at the vicinity of strained and elongated prior β grains, giving a necklace appearance. The findings are consistent with the reported results for hot working of IMI834, TA15 and TC11 Titanium alloy, maintaining the existence of recrystallized equiaxed grains due to deformation-induced dynamic recrystallization [25–28]. The appearance of dynamically recrystallized grains at the prior β grain boundary or intragrain crystallographic features (inclusions or shear bands) can be attributed to the requirement to attain critical dislocation density for nucleation of recrystallized grains [29].

(a) T=1248 K, $\dot{\epsilon}=10^{-3}\mathrm{s}^{-1}$ (b) 1248 K, $\dot{\epsilon}=10^{-2}\mathrm{s}^{-1}$ (c) T=1248 K, $\dot{\epsilon}=1^{-1}\mathrm{s}^{-1}$

(d) T=1248 K, $\dot{\epsilon}=1\mathrm{s}^{-1}$ (e) T=1248 K, $\dot{\epsilon}=10\mathrm{s}^{-1}$

Fig. 6 OM images of microstructure of specimens deformed to 0.69 true strain. The compression axis is vertical

(a) T=1298 K, $\dot{\epsilon}=10^{-3}\mathrm{s}^{-1}$ (b) T=1298 K, $\dot{\epsilon}=10^{-2}\mathrm{s}^{-1}$ (c) T=1298 K, $\dot{\epsilon}=1^{-1}\mathrm{s}^{-1}$

(d) T=1298 K, $\dot{\epsilon}=1\mathrm{s}^{-1}$ (e) T=1298 K, $\dot{\epsilon}=10\mathrm{s}^{-1}$

Fig. 7 OM images of microstructure of specimens deformed to 0.69 true strain. The compression axis is vertical

This further helps to relate it to a predominant dynamic process leading to recrystallization. The necklace structure or the microstructural inhomogeneity is a result of preferential recrystallization along the high strain regions (e.g. grain boundary) accompanied by low driving potential for recrystallization in grain interiors because of dominant recovery process [30]. Thus, from the above observation and reported literature, it can be inferred that for uniform recrystallization of the structure, low strain rates and sufficient final strain is necessary. This limitation for dynamic

Table 1 Variation in microstructure with varying temperature and strain rate of deformation

| Temperature (K)	Strain rate	Microstructural feature
1098	10^{-3} s^{-1}	Globular + lamellae bending
	10^{-2} s^{-1}	Globular + lamellae bending
	10^{-1} s^{-1}	Globular+ lamellae bending
	1 s^{-1}	Lamellae kinking
	10 s^{-1}	Localized flow bands
1148	10^{-3} s^{-1}	Globular + lamellae bending
	10^{-2} s^{-1}	Globular + lamellae bending
	10^{-1} s^{-1}	Globular+ lamellae bending
	1 s^{-1}	Lamellae kinking
	10s^{-1}	Lamellae bending
1198	10^{-3} s^{-1}	Diffused α
	10^{-2} s^{-1}	Lamellae kinking + diffused α
	10^{-1} s^{-1}	Lamellae kinking + diffused α
	1 s^{-1}	Lamellae kinking + diffused α
	10s^{-1}	Diffused α + α' martensite
1248	10^{-3} s^{-1}	Equiaxed β grains + martensite
	10^{-2} s^{-1}	Equiaxed β grains + martensite + elongated prior β grains
	10^{-1} s^{-1}	Equiaxed β grains + martensite + elongated prior β grains
	1 s^{-1}	Equiaxed β grains + martensite + elongated prior β grains
	10s^{-1}	Elongated prior β grains + martensite
1298	10^{-3} s^{-1}	Equiaxed β grains + martensite
	10^{-2} s^{-1}	Equiaxed β grains + martensite + elongated prior β grains
	10^{-1} s^{-1}	Equiaxed β grains + martensite + elongated prior β grains
	1 s^{-1}	Equiaxed β grains + martensite + elongated prior β grains
	10s^{-1}	Elongated prior β grains + martensite

recrystallization is related to the difficulty in achieving high dislocation density. β phase presents high self-diffusivity and aids in dislocation mobility; this results in reduced stored energy via dynamic recovery. This further results in the homogenization of dislocation substructure and subsequently reduces the driving force for recrystallization [31]. As for the specimens deformed at 1298 K, the mechanism of microstructure evolution was the same as mentioned earlier, but with a larger prior β grains. An increase in dynamically recrystallized grain size has been reported for hot working of Ti–6Al–4V at a strain rate of 10^{-3} s^{-1} with increasing temperature of hot working [32]. The following observation is in agreement with the reported work on the hot deformation of Ti–6Al–4V in uniphase β region [18, 29]. Table 1 enlists different microstructure for varying temperature and deformation modes.

4 Processing map

A processing map is a stencil used to draft a hot-working routine for metals and alloys to obtain a defect-free and homogeneous microstructure. The approach of drawing processing maps rests on a dynamic material model (DMM) reported by [33, 34] and [35] has been widely applied for titanium alloys [36, 37]. It assumes specimen to be a power dissipator. Total power spent (P) during deformation is defined by power dissipation function (G) and microstructural change function (J) and are related mathematically as:

$$P = G + J = \int_0^{\bar{\sigma}} \dot{\bar{\epsilon}} \, \mathrm{d}\bar{\sigma} + \int_0^{\bar{\epsilon}} \bar{\sigma} \, \mathrm{d}\dot{\bar{\epsilon}} \qquad (1)$$

It is known that at high temperature, material flow is a function of strain rate and is represented by strain rate sensitivity (m), as shown in the equation below.
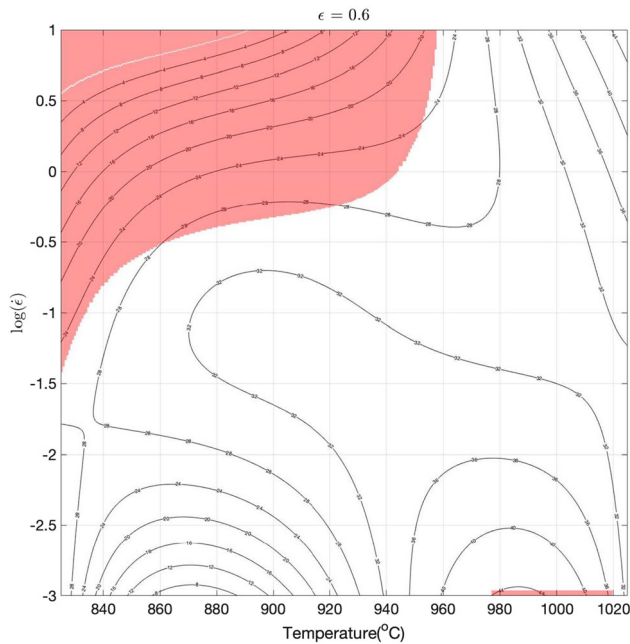
Fig. 8 Processing map of Ti–5Al–3Mo–1.5V at $\epsilon = 0.6$

$$\frac{\mathrm{d}J}{\mathrm{d}G} = \frac{\dot{\bar{\epsilon}}\mathrm{d}\bar{\sigma}}{\bar{\sigma}\mathrm{d}\dot{\bar{\epsilon}}} = \frac{\dot{\bar{\epsilon}}\bar{\sigma}\mathrm{d}\ln\bar{\sigma}}{\bar{\sigma}\dot{\bar{\epsilon}}\mathrm{d}\ln\dot{\bar{\epsilon}}} \approx \frac{\Delta\log_{10}\bar{\sigma}}{\Delta\log_{10}\dot{\bar{\epsilon}}} = m \tag{2}$$

The function contributing to the microstructural change can be simplified for a given temperature to:

$$J = \frac{m\bar{\sigma}\dot{\bar{\epsilon}}}{m+1} \tag{3}$$

J attains it's maximum value for $m = 1$ and acts as a linear dissipator.

$$J_{\max} = \frac{\bar{\sigma}\dot{\bar{\epsilon}}}{2} \tag{4}$$

A power dissipation profile represented in temperature versus strain rate graph is used to depict the power expenditure out of total input power $(\bar{\sigma} \cdot \dot{\bar{\epsilon}})$ in microstructural change rather than heat generation. This expenditure is compared to that of ideal linear dissipator and represented by a dimensionless quantity 'η' (Power dissipation efficiency). Hot working in high η regime of power dissipation map is considered favourable.

$$\eta = \frac{2m}{m+1} \tag{5}$$

Using an instability criterion, $\xi(\dot{\bar{\epsilon}})$, a instability map is generated and superimposed over the power dissipation map. The instability criterion proposed was further based on the extremum principle of irreversible thermodynamics. Unstable zones like the adiabatic shear bands, slip localization, grain boundary cavitation initiated crack formation are represented by this instability map. Region

corresponding to negative values of ξ in Eq. (6) represents the unstable zone.

$$\xi(\dot{\epsilon}) = \frac{\partial\ln(m/m+1)}{\partial\ln\dot{\epsilon}} \tag{6}$$

In this test, stress versus strain values from high temperature deformation studies are used to calculate η, m and ξ which are then used in evaluating the processing map at the strain level 0.69. In the map shown in Fig. 8, white coloured regions show the stable zones, and the red coloured regions represent the unstable zones. Highest value of η was found to be around 40–44% at 10^{-3} s^{-3} and 1248 K. Subsequently, the microstructure in the before-mentioned conditions depicts dynamically recrystallized defect-free grains. For the specimens deformed at higher temperature and at a higher strain rate, necklace structure suggested initiation of selective DRX on the deformed prior β grain boundaries. For intermediate temperatures and low strain rate, shear bands and absence of DRX was observed. Considering Eqs: 5, 6 and correlating with the microstructures, safe working window for the alloy is 1248 K and 10^{-3} s^{-1}.

5 Constitutive equations

An empirical constitutive model was proposed by Sellar and McTegart [38, 39] to characterize the high-temperature deformation characteristics of different metals. It is a phenomenological model based on continuum mechanics and does not explicitly address the microstructural evolution. Though the model does not account for texture or grain size refinement, it has served as a special tool for material design and hot-working activation energy estimations. The physical behaviour of the alloy during and after the deformation is modelled based on material constants. For this work, Arrhenius mode is employed to establish a correlation between temperature, flow stress, strain rate, strain and deformation condition by calculating Zener–Holloman parameter (z) [40].

$$Z = \dot{\epsilon}\exp\left(\frac{Q}{RT}\right) = f(\sigma) = \begin{Bmatrix} A\exp(\beta\alpha) \\ A'\sigma^{n'} \\ A''[\sinh(\alpha\sigma)]^n \end{Bmatrix} \tag{7}$$

With the use of three different functions involving hyperbolic, exponential and power relationships, Z can be correlated with flow stress as shown in Eq. (7) in which α and β are prefactors for the flow stress and A, A', A'', n' are material constants. The value assigned to the stress σ can either be that of flow stress at a given strain level or the maximum value of flow stress or the steady state stress.

The choice is based on the active DRX mechanism by choosing the maximum value of the flow stress under given temperature and strain rate the expression for the above-mentioned material parameters and the activation energy (Q) are obtained as follows in Eq. (8). Further details of the derivation can be found in 34 35.

$$\ln(\dot{\epsilon}) + \frac{Q}{R}\left(\frac{1}{T}\right) = \begin{Bmatrix} \ln(A) + \beta\sigma \\ \ln(A') + n'\ln(\sigma) \\ \ln(A'') + n\ln[\sinh(\alpha\sigma)] \end{Bmatrix} \qquad (8)$$

$$\beta = \left[\frac{\partial\ln\dot{\epsilon}}{\partial\sigma}\right]_T ; n' = \left[\frac{\partial\ln\dot{\epsilon}}{\partial\ln\sigma}\right]_T ; n = \left[\frac{\partial\ln\dot{\epsilon}}{\partial\ln[\sinh(\alpha\sigma)]}\right]_T \qquad (9)$$

β and n' is obtained from the slopes of $\ln\dot{\epsilon}$ versus σ (Fig. 10b) and $\ln\dot{\epsilon}$ versus $\ln\sigma$ (Fig. 10a), respectively. σ, the stress multiplier is obtained from β and n' ($\alpha = \beta/n'$). Linear regression is utilized to calculate the average β, n' and n values from Eq. (8) with goodness of fit (R^2) > 0.9. Amongst all the reported phenomenological models, sine hyperbolic function (Eq. 7) is employed for the complete stress range and was utilized for the activation energy (Q).

$$Q = R\left[\frac{\partial\ln\dot{\epsilon}}{\partial\ln[\sinh(\alpha\sigma)]}\right]_T \left[\frac{\partial\ln(\sinh(\alpha\sigma_p))}{\partial\left(\frac{1}{T}\right)}\right]_\epsilon \qquad (10)$$

The values of β, n', n, α and Q for different phases are mentioned in the table.

The apparent hot-working activation energy Q, is found to be 636 kJ/mol in the $\alpha + \beta$ regime. The obtained apparent activation energy for hot working is higher than what is required for the self-diffusion of α-Ti (169 kJ/mol) and β-Ti (153 kJ/mol) [39, 41]. The occurrence of high apparent activation energy can be attributed to the dynamic globularization or breakup of lamellae ensuing deformation in the $\alpha + \beta$ regime [9]. High apparent activation energy has been previously reported for titanium alloys with lamellar starting microstructure viz. Ti-17 (488.86 kJ/mol) [42], Ti60 (653 kJ/mol) [43] and Ti–6Al–4V (437 kJ/mol) [30]. For deformation in the β phase field an activation energy of 379 kJ/mol was witnessed, which is considerably higher than the reported self-diffusion barrier for β-Ti (153 kJ/mol) [30]. Articles reporting similar results attributed this observation to dynamic recrystallization phenomena. For single-phase alloys, it has been extensively reported that the rate controlling step was dynamic recrystallization in case of high activation energy as opposed to dynamic recovery initiated by dislocation glide and dislocation climb [28, 44]. Figure 9 shows a schematic representation of different deformation mechanisms active for different temperature and strain rates.
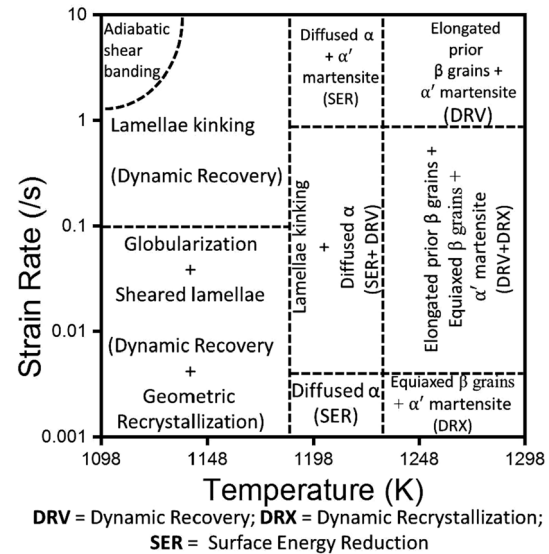

Fig. 9 Phase transformation/deformation mechanism for different temperature and strain rate

Table 2 Values of the material constants, work hardening exponents and hot-working activation energy obtained from the graphs depicted in Fig. 10

Phase	Parameter	Value
β titanium	β	0.13
	n'	4.82
	α	0.27
	n	3.6
	Q	379 kJ/mol
α titanium	β	0.08
	n'	7.07
	α	0.0.01
	n	5.16
$\alpha + \beta$	Q	636 kJ/mol

6 Conclusion

A detailed analysis of the concurrent effect of varying temperature and deformation conditions on microstructure was conducted. It was observed that for lower two-phase region, the size of globules were inversely proportional to the strain rate and its formation concentrated near the lamellae kink. With increasing temperature, localized $\beta \rightarrow \alpha$ transformation dominated and a complete martensitic structure was obtained for above β transus regime. Furthermore, dynamic recrystallization was prominent near the prior β grain boundaries, and the size of these recrystallized grains was directly and inversely proportional to temperature and strain rate, respectively. Processing maps of Ti–5Al–3Mo–1.5V dual-phase titanium alloy helped in
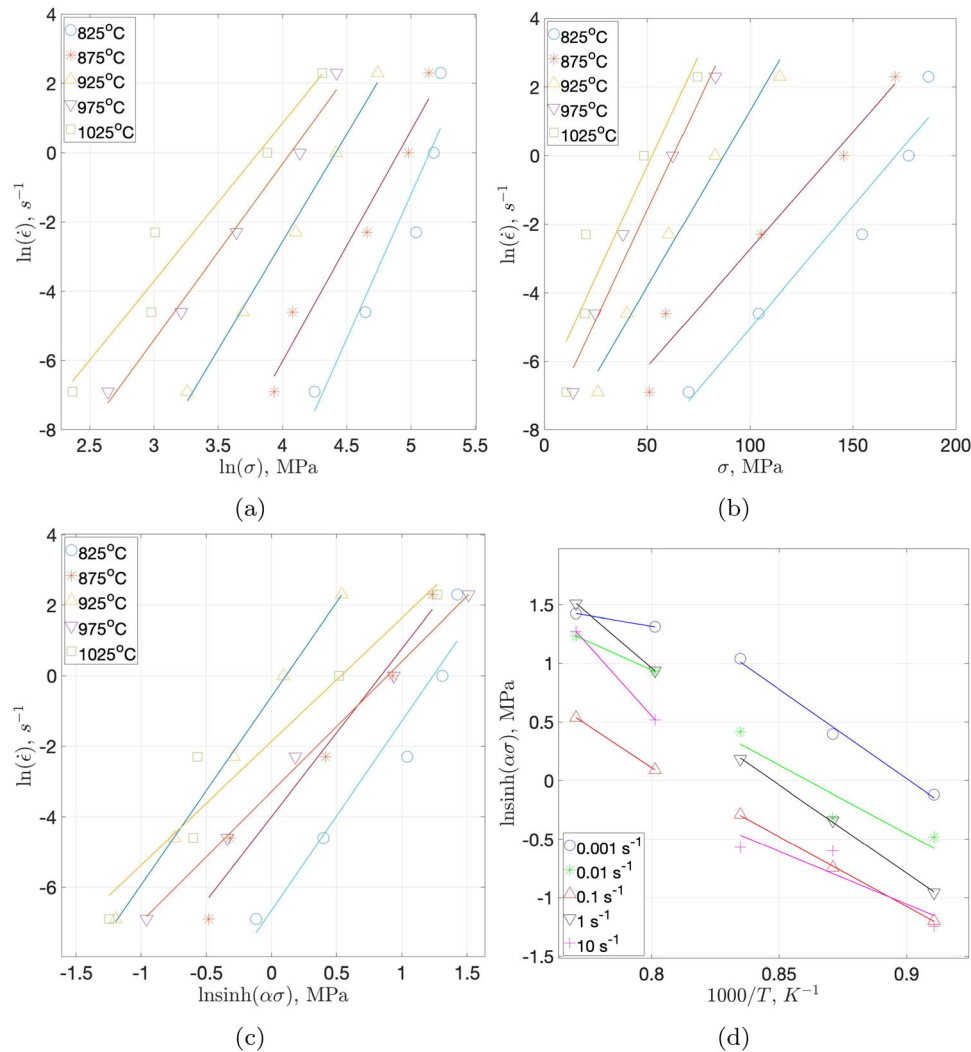
Fig. 10 **a** Plot of $\ln\dot{\epsilon}$ versus $\ln\sigma$, **b** Plot of $\ln\dot{\epsilon}$ versus σ to calculate α **c** slope of $\log\dot{\epsilon}$ versus $\ln\sinh(\alpha\sigma)$ gives work hardening exponent n and **d** plot of $\ln\sinh(\alpha\sigma)$ versus $(1000/T)$ to compute apparent hot-working activation energy, Q (kJ/mol)

identifying the optimum hot working condition to be 1248 K and 10^{-3} s^{-1}. Hot-working activation energy higher than self-diffusivity in α and β phases indicated that lamellae breakup and dynamic recrystallization is the major deformation mechanism in the respective phases. Finally, dynamic material model was successfully employed to find safe working regime for the alloy.

References

1. Moiseyev, V.: Titanium Alloys: Russian Aircraft and Aerospace Applications. Taylor and Francis, Abingdon-on-Thames (2005)
2. Syed, F.W., Anil Kumar, V., Gupta, R.K., Kanjarla, A.K.: Role of microstructure on the tension/compression asymmetry in a two-phase Ti–5Al–3Mo–1.5V titanium alloy. J. Alloys. Compd. **795**, 151 (2019). https://doi.org/10.1016/J.JALLCOM.2019.04.272
3. Shell, E.B., Semiatin, S.L.: Effect of initial microstructure on plastic flow and dynamic globularization during hot working of Ti–6Al–4V. Metall. Mater. Trans. A **30**(12), 3219 (1999). https://doi.org/10.1007/s11661-999-0232-4
4. Stefansson, N., Semiatin, S.L.: Mechanisms of globularization of Ti–6Al–4V during static heat treatment. Metall. Mater. Trans. A **34**(3), 691 (2003). https://doi.org/10.1007/s11661-003-0103-3
5. Ardell, A.J.: Microstructural stability at elevated temperatures. J. Eur. Ceram. Soc. **19**(13–14), 2217 (1999). https://doi.org/10.1016/S0955-2219(99)00094-1

6. Nakagawa, Y.G., Weatherly, G.C., Ho, E.: Coarsening of lamellar structures at elevated temperatures. Mater. Trans. Jpn. Inst. Metals **15**, 114 (1974). https://doi.org/10.2320/matertrans 1960.15.114

7. Korshunov, A.A., Enikeev, F.U., Mazurskij, M.I., Salishchev, G.A., Muravlev, A.V., Chistyakov, P.V., Dmitriev, O.V.: Effect of the method of high-temperature loading on the transformation of lamellar structure in titanium alloy VT9Document details, Izvestia Akademii nauk SSSR. Metally **3**, 121 (1994)

8. Semiatin, S.L., Seetharaman, V.: Plastic flow, microstructure evolution, and defect formation during primary hot working of titanium and titanium aluminide alloys with lamellar colony microstructures. Philos. Trans. R. Soc. A **357**(1756), 1487 (1999). https://doi.org/10.1098/rsta.1999.0386

9. Seshacharyulu, T., Medeiros, S., Frazier, W., Prasad, Y.: Microstructural mechanisms during hot working of commercial grade Ti–6Al–4V with lamellar starting structure. Mater. Sci. Eng. A **325**(1–2), 112 (2002). https://doi.org/10.1016/S0921-5093(01)01448-4

10. Sellars, C.M.: Recrystallization of metals during hot deformation. Philos. Trans. R. Soc. A Math. Phys. Eng. Sci. **288**(1350), 147 (1978). https://doi.org/10.1098/rsta.1978.0010

11. Poliak, E.I., Jonas, J.J.: Initiation of dynamic recrystallization in constant strain rate hot deformation. ISIJ Int. **43**(5), 684 (2003). https://doi.org/10.2355/isijinternational.43.684

12. Ding, R., Guo, Z.: Coupled quantitative simulation of microstructural evolution and plastic flow during dynamic recrystallization. Acta Mater. **49**(16), 3163 (2001). https://doi.org/10.1016/S1359-6454(01)00233-6

13. Kugler, G., Turk, R.: Modeling the dynamic recrystallization under multi-stage hot deformation. Acta Mater. **52**(15), 4659 (2004). https://doi.org/10.1016/j.actamat.2004.06.022

14. Chen, H.Q., Cao, C.X., Guo, L., Lin, H.: Hot deformation mechanism and microstructure evolution of TC11 titanium alloy in β field. Trans. Nonferrous Metals Soc. China **18**(5), 1021 (2008). https://doi.org/10.1016/S1003-6326(08)60175-2

15. Semiatin, S., Seetharaman, V., Weiss, I.: Flow behavior and globularization kinetics during hot working of Ti–6Al–4V with a colony alpha microstructure. Mater. Sci. Eng. A **263**(2), 257 (1999). https://doi.org/10.1016/S0921-5093(98)01156-3

16. Miller, R., Bieler, T., Semiatin, S.: Flow softening during hot working of Ti–6Al–4V with a lamellar colony microstructure. Scripta Mater. **40**(12), 1387 (1999). https://doi.org/10.1016/S1359-6462(99)00061-5

17. Gao, P., Fu, M., Zhan, M., Lei, Z., Li, Y.: Deformation behavior and microstructure evolution of titanium alloys with lamellar microstructure in hot working process: a review. J. Mater. Sci. Technol. **39**, 56 (2020). https://doi.org/10.1016/j.jmst.2019.07.052

18. Ding, R., Guo, Z., Wilson, A.: Microstructural evolution of a Ti–6Al–4V alloy during thermomechanical processing. Mater. Sci. Eng. A **327**(2), 233 (2002). https://doi.org/10.1016/S0921-5093(01)01531-3

19. Semiatin, S.L., Thomas, J.F., Dadras, P.: Processing-microstructure relationships for Ti–6Al–2Sn–4Zr–2Mo–0.1Si. Metall. Trans. A **14**(11), 2363 (1983). https://doi.org/10.1007/BF02663312

20. Weiss, I., Froes, F.H., Eylon, D., Welsch, G.E.: Modification of alpha morphology in Ti–6Al–4V by thermomechanical processing. Metall. Trans. A **17**(11), 1935 (1986). https://doi.org/10.1007/BF02644991

21. Fan, X.G., Zheng, H.J., Zhang, Y., Zhang, Z.Q., Gao, P.F., Zhan, M., Liu, J.: Acceleration of globularization during interrupted compression of a two-phase titanium alloy. Mater. Sci. Eng. A **720**, 214 (2018). https://doi.org/10.1016/j.msea.2018.02.026

22. Song, H.W., Zhang, S.H., Cheng, M.: Dynamic globularization kinetics during hot working of a two phase titanium alloy with a colony alpha microstructure. J. Alloys. Compd. **480**(2), 922 (2009). https://doi.org/10.1016/J.JALLCOM.2009.02.059

23. Weiss, I., Sakai, T., Jonas, J.J.: Effect of test method on transition from multiple to single peak dynamic recrystallization. Metal Sci. **18**(2), 77 (1984). https://doi.org/10.1179/030634584790420249

24. Furuhara, T., Poorganji, B., Abe, H., Maki, T.: Dynamic recovery and recrystallization in titanium alloys by hot deformation. JOM **59**(1), 64 (2007). https://doi.org/10.1007/s11837-007-0013-8

25. Wang, X.X., Zhan, M., Gao, P.F., Ma, P.Y., Yang, K., Lei, Y.D., Li, Z.X.: Deformation mode dependent mechanism and kinetics of dynamic recrystallization in hot working of titanium alloy. Mater. Sci. Eng. A **772**, 138804 (2020). https://doi.org/10.1016/j.msea.2019.138804

26. Ding, R., Guo, Z.: Microstructural evolution of a Ti–6Al–4V alloy during β-phase processing: experimental and simulative investigations. Mater. Sci. Eng. A **365**(1–2), 172 (2004). https://doi.org/10.1016/j.msea.2003.09.024

27. Weiss, I., Semiatin, S.: Thermomechanical processing of alpha titanium alloys-an overview. Mater. Sci. Eng. A **263**(2), 243 (1999). https://doi.org/10.1016/S0921-5093(98)01155-1

28. Zhang, X., Li, M., Li, H., Luo, J., Su, S., Wang, H.: Deformation behavior in isothermal compression of the TC11 titanium alloy. Mater. Des. **31**(6), 2851 (2010). https://doi.org/10.1016/j.matdes.2009.12.051

29. Wanjara, P., Jahazi, M., Monajati, H., Yue, S.: Influence of thermomechanical processing on microstructural evolution in near-α alloy IMI834. Mater. Sci. Eng. A **416**(1–2), 300 (2006). https://doi.org/10.1016/J.MSEA.2005.10.042

30. Weiss, I., Semiatin, S.: Thermomechanical processing of beta titanium alloys—an overview. Mater. Sci. Eng. A **243**(1–2), 46 (1998). https://doi.org/10.1016/S0921-5093(97)00783-1

31. Guo, Z., Baker, T.: On the microstructure and thermomechanical processing of titanium alloy IMI685. Mater. Sci. Eng. A **156**(1), 63 (1992). https://doi.org/10.1016/0921-5093(92)90416-X

32. Honarmandi, P., Aghaie-Khafri, M.: Hot deformation behavior of Ti–6Al–4V alloy in β phase field and low strain rate. Metallogr. Microstruct. Anal. **2**(1), 13 (2013). https://doi.org/10.1007/s13632-012-0052-6

33. Prasad, Y.V.R.K., Seshacharyulu, T.: Modelling of hot deformation for microstructural control. Int. Mater. Rev. **43**(6), 243 (1998). https://doi.org/10.1179/imr.1998.43.6.243

34. Jaladurgam, N.R., Kanjarla, A.K.: Hot deformation characteristics and microstructure evolution of Hastelloy C-276. Mater. Sci. Eng. A **712**, 240 (2018). https://doi.org/10.1016/J.MSEA.2017.11.056

35. Prasad, Y.V.R.K., Rao, K.P., Sasidhara, S.: Hot Working Guide: A Compendium of Processing Maps, 2nd edn. ASM International, Russell Township (2015)

36. Prasad, Y., Seshacharyulu, T.: Processing maps for hot working of titanium alloys. Mater. Sci. Eng. A **243**(1–2), 82 (1998). https://doi.org/10.1016/S0921-5093(97)00782-X

37. Sheikhali, A.H., Morakkabati, M.: Hot working of SP-700 titanium alloy with lamellar $\alpha + \beta$ starting structure using a processing map. Int. J. Mater. Res. **111**(4), 297 (2020). https://doi.org/10.3139/146.111881

38. Sellars, C., McTegart, W.: On the mechanism of hot deformation. Acta Metall. **14**(9), 1136 (1966). https://doi.org/10.1016/0001-6160(66)90207-0

39. Jonas, J.J., Sellars, C.M., McTegart, W.J.: Strength and structure under hot-working conditions. Metall Rev **14**(1), 1 (1969). https://doi.org/10.1179/mtlr.1969.14.1.1

40. Zener, C., Hollomon, J.H.: Effect of strain rate upon plastic flow of steel. J. Appl. Phys. **15**(1), 22 (1944). https://doi.org/10.1063/1.1707363

41. Flower, H.M.: Microstructural development in relation to hot working of titanium alloys. Mater. Sci. Technol. (U.K.) **6**(11), 1082 (1990). https://doi.org/10.1179/mst.1990.6.11.1082

42. Wang, K.X., Zeng, W.D., Zhao, Y.Q., Lai, Y.J., Zhang, X.M., Zhou, Y.G.: Flow behaviour and microstructural evolution of Ti-17 alloy with lamellar microstructure during hot deformation in $\alpha+\beta$ phase field. Mater. Sci. Technol. **27**(1), 21 (2011). https://doi.org/10.1179/174328409X463252

43. Jia, W., Zeng, W., Zhou, Y., Liu, J., Wang, Q.: High-temperature deformation behavior of Ti60 titanium alloy. Mater. Sci. Eng. A **528**(12), 4068 (2011). https://doi.org/10.1016/j.msea.2011.01.113

44. Ghasemi, E., Zarei-Hanzaki, A., Farabi, E., Tesař, K., Jäger, A., Rezaee, M.: Flow softening and dynamic recrystallization behavior of BT9 titanium alloy: a study using process map development. J. Alloys. Compd. **695**, 1706 (2017). https://doi.org/10.1016/J.JALLCOM.2016.10.322